M. Selva[1,*], B. Aiazzi, F. Butera, L. Chiarantini and S. Baronti, "**Hyper-Sharpening: A First Approach on SIM-GA Data**," in IEEE Journal of Selected Topics in Applied Earth Observations and Remote Sensing, vol. 8, no. 6, pp. 3008-3024, June 2015, doi: 10.1109/JSTARS.2015.2440092

[1] "Nello Carrara" Institute of Applied Physics, National Research Council, 50019 Sesto Fiorentino (FI), Italy.
* Correspondence: m.selva@ifac.cnr.it

To cite this paper:

M. Selva, B. Aiazzi, F. Butera, L. Chiarantini and S. Baronti, "Hyper-Sharpening: A First Approach on SIM-GA Data," in IEEE Journal of Selected Topics in Applied Earth Observations and Remote Sensing, vol. 8, no. 6, pp. 3008-3024, June 2015, doi: 10.1109/JSTARS.2015.2440092.

@ARTICLE{7134741,
author={Selva, Massimo and Aiazzi, Bruno and Butera, Francesco and Chiarantini, Leandro and Baronti, Stefano},
journal={IEEE Journal of Selected Topics in Applied Earth Observations and Remote Sensing},
title={Hyper-Sharpening: A First Approach on SIM-GA Data},
year={2015},
volume={8},
number={6},
pages={3008-3024},
doi={10.1109/JSTARS.2015.2440092}}

Hyper-Sharpening: A First Approach on SIM-GA Data

Massimo Selva, Bruno Aiazzi, *Member IEEE*, Francesco Butera, Leandro Chiarantini, Stefano Baronti, *Member IEEE*

***Abstract*—This paper aims at defining a new paradigm in remote sensing image fusion: hypersharpening. In fact, due to the development of new instruments, thinking only in terms of pansharpening is reductive. Even though some terms as hyperspectral pansharpening already exist, there is not a suitable definition when multispectral/hyperspectral data are utilized as source to extract spatial details. After defining the hypersharpening framework, we draw the readers' attention to its peculiar characteristics, by proposing and evaluating two hypersharpening methods. Experiments are carried out on the data produced by the updated version of SIM-GA imager, designed by Selex ES, which is composed by a panchromatic camera and two spectrometers in the VNIR and SWIR spectral ranges, respectively. Due to the different resolution factors among Panchromatic, VNIR and SWIR data sets, we can apply hypersharpening to fuse SWIR data to VNIR resolution. Comparisons of hypersharpening with "traditional" pansharpening show hypersharpening is more effective.**

***Index Terms*—Dimensionality Reduction, Hypersharpening, Hyperspectral, Image Fusion, Pansharpening, Remote Sensing.**

I. INTRODUCTION

A. The past and the present: pansharpening

Pansharpening is a branch of data fusion, more specifically of image fusion, which has been receiving an ever-increasing attention in the remote sensing community. Modern spaceborne imaging sensors operate in a variety of ground scales and spectral bands and consequently provide huge volumes of data with complementary spatial and spectral resolutions. Constraints on the signal to noise ratio (SNR) require that the spatial resolution is worse, if the desired spectral resolution is better. On the other end, a high spatial resolution would be important when spectral diversity is required. Thus, it would be desirable to perform a spatial resolution enhancement of the lower resolution multispectral (MS) data or, equivalently, to increase the spectral resolution of the unique panchromatic image (Pan) exhibiting a higher ground resolution with no spectral information.

M. Selva, B. Aiazzi and S. Baronti are with the Instituto di Fisica Applicata "Nello Carrara", CNR Area della Ricerca di Firenze, 50019 Sesto Fiorentino (FI), Italy. (e-mail: {m.selva b.aiazzi s.baronti }@ifac.cnr.it).

F. Butera and L. Chiarantini are with Selex ES, Via A. Einstein, 35, 50013 Campi Bisenzio, Florence, Italy.

Acknowledgment: This work was carried out with the support of the Agenzia Spaziale Italiana (ASI), contract n. CNR-IFAC/SOASAR/111213. SIM-GA data are acquired during an airborne survey (May 2013) on Viareggio (Italy) conducted by CISAM, Information Engineering Dept. of Pisa University and Selex ES.

Progress in pansharpening methods has been substantially motivated by advances in spaceborne instruments. Pansharpening methods have been progressively developed since the launch of SPOT-1 (1986), which was the first system featuring two MS bands together with one Pan. Over the last 30 years, pansharpening has followed the evolution of satellite technology, passing from 3 MS bands + Pan (SPOT 2, 3, 4, 5), 6 MS bands + Pan (Landsat ETM+), 4 MS bands + Pan (IKONOS-2, QuickBird-2, GeoEye-1, GeoEye-2, Pléiades), up to 8 MS bands + Pan (WorldView-2). Most instruments launched during the last decade exhibit a ratio of scales between Pan and MS equal to four, instead of two, as earlier missions.

According to [1], [2] and [3], the majority of image fusion methods can be categorized into two classes: component substitution (CS) and multiresolution analysis (MRA). The two classes differ on how spatial details are extracted from the Pan image. According to this classification, all methods belonging to CS and MRA classes exhibit specific characteristics. CS methods produce spatially sharper fused products while MRA fused images appear of better spectral quality. CS and MRA methods exhibit also a different behavior when the data are affected by such effects as aliasing and misregistration [2].

MRA class contains the techniques employing linear space-invariant digital filtering of the Pan image to extract the spatial details to be added to the MS bands. Also methods related to ARSIS concept (Amélioration de la Résolution Spatiale par Injection de Structures), originally employing the decimated wavelet transform (DWT) [4], are part of this group [5], [6], [7].

CS family groups the techniques that yield the spatial details as a pixel difference between the Pan image and a nonzero-mean component obtained from a spectral transformation of the MS bands, without any spatial filtering of the Pan. Thus, intensity–hue–saturation (IHS) and its variants [8], [9], Brovey transform (BT) [10], and principal component analysis (PCA) [11] are in this group. These methods are equivalent to the substitution of such a component with the Pan image followed by reverse transformation to produce the sharpened MS bands [12], [13], [14].

Regardless of how spatial details have been obtained, their injection into the interpolated MS bands may be weighted by suitable gains, different for each band, possibly space-varying, i.e. a different gain at each pixel. Algorithms featuring context-adaptive, i.e. local, models generally perform better than schemas based on models fitting each band globally [1].

This classification excludes the methods based on the sparse representation of the images. The natural images, in fact, satisfy a sparse model, that is, they can be seen as the linear combination of few elements of a dictionary or atoms. Sparse models are at the basis of compressed sensing [15]. In the pansharpening field, the pioneering paper [16] formulated the remote sensing imaging formation model as a linear transform corresponding to the measurement matrix in the compressing sensing theory [15]. In this context, the high-resolution Pan and low-resolution MS images are referred as measurements, and the high-resolution MS images can be recovered by applying sparsity regularization. The generation of the dictionary is the key problem of all pansharpening approaches based on compressed sampling. In [16], the dictionary is generated by randomly sampling raw patches from high-resolution MS satellite images. In [17], the sparse coefficients of the Pan image and low-resolution MS image are obtained by orthogonal matching pursuit algorithm. In [18], the Sparse Fusion of Images (SparseFI) algorithm explores the sparse representation of multispectral image patches in a dictionary trained only from the panchromatic image at hand. Furthermore, it does not assume for the Pan image any spectral composition model that could imply a relationships between the dictionaries of Pan and MS.

With the launch in 2001 of Earth Observer 1 (EO-1) satellite, new perspectives in pansharpening were opened. This satellite, in fact, hosts the Advanced Land Imager (ALI) MS scanner and the Hyperion imaging spectrometer. ALI acquires nine MS channels and a Pan image with a spatial sampling interval (SSI) of 30 m and 10 m, respectively. Hyperion is a hyperspectral (HS) imager capable of observing 220 spectral bands (0.4 to 2.5 nm) with 30 m SSI. The swaths of ALI and Hyperion are partially overlapped, in such a way that there is a part of the scene in which Pan, MS and HS data are simultaneously available. On this scene, fusion algorithms can be developed and applied to spatially enhance an HS image for a 3:1 scale ratio, thus extending pansharpening to HS data.

In this framework, HS resolution enhancement, or HS sharpening, refers to the joint processing of the data in order to synthesize an HS product that ideally exhibits the spectral characteristics of the observed HS image at the spatial resolution, and hence sampling, of the higher resolution image.

Indeed, many developments of spatial resolution enhancement of HS data have been rough extensions of some of MS pansharpening algorithms we have just reviewed. In this regard, some interesting papers have been published.

A very specific approach to HS data fusion was proposed for the first time in [19]. It is based on the application of Spectral Mixing Models. This approach starts with conventional unmixing to generate fractional images and applies a constrained optimization technique to spatially locate the endmembers at high resolution. However, the results were limited to the synthetic data where the endmembers are known a *priori*. The same authors conducted more in-depth testing on this method and presented results in [20]. In [21], a maximum a posteriori (MAP) estimation method was introduced. The cost function derived from MAP is solved by using a stochastic mixing model (SMM) of the underlying spectral scene. This cost function simultaneously optimizes the estimated hyperspectral scene relative to the observed HS and Pan imagery, as well as the local statistics of the spectral mixing model. More recently, in [22], an approach based on linear spectral mixture model has been implemented by using the coupled nonnegative matrix factorization (CNMF) unmixing. Both HS and MS data are alternately unmixed into endmember and abundance matrices. Sensor observation models that relate the two data sets are built into the initialization matrix of each NMF unmixing procedure. However, this method is physically straightforward, but computationally expensive and little intuitive. This approach was also experimented on Hyperspectral Imager Suite (HISUI) simulated data [23].

The method proposed in [24] employed MAP estimation based on a spatially varying statistical model to enhance the HS image resolution; the developed framework was validated only for pansharpening but allowed for any number of spectral bands in both the MS and HS images. This bayesian approach has been further improved by the same authors in [25], by investigating and demonstrating the advantages of using a high resolution MS image as source for a MS/HS fusion. Based on [24], the paper [26] proposed an approach that works in the wavelet domain assuming a joint normal model for the images and an additive noise imaging model for the HS data. This approach, however, is time consuming.

Among the HS methods that are extensions of conventional pansharpening algorithms, we mention [27]. This approach modifies the Spectral Distortion Minimization (SDM) method [28], introducing a multiplicative factor β aimed at magnifying or damping the spectral vector that constitutes the spatial enhancement. The coefficient β is chosen in order to minimize the spatial distortion according to the Quality No Reference (QNR) protocol [29]. In [30], the authors proposed a fusion technique that combines dimensionality reduction carried out by using non-linear principal component analysis (NLPCA) with the pansharpening approach in the indusion variant [31]. In [32], an approach to fuse hyperspectral and multispectral image was presented. The key idea is dividing the spectrum of HS data into several regions and fusing HS and MS images in each region by choosing a MS image in the role of Pan. Due to its structure, this framework allows most of pansharpening algorithms to be extended to HS and MS fusion.

B. Towards the future: hypersharpening

We felt particulary gratified when we introduced the new word "hyper-sharpening" at the WHISPERS conference in June 2014 [38].

Since technological developments were often replacing or complementing Pan cameras with MS/HS instruments [33], the term pansharpening was becoming no longer suitable to indicate the traditional methods when employed to spatially enhance MS/HS data sets.

Pansharpening, in fact, implied or should have implied the existence of *one single* image at high spatial resolution that could be used to enhance the sharpness of a certain number of MS/HS bands at lower resolution.

Similarly for the passage from multispectral to hyperspectral data, we proposed thinking in terms of "hyper-sharpening".

This new term pointed out that the spatially enhancing *one single* image could be in the reality *a set* (potentially a *hyperspectral cube*) of bands.

When a new idea is proposed, very rarely it is completely outside the context. Some other groups in fact, were studying the potentiality of fusion between a multispectral and hyperspectral datasets. Starting from the previous works [24], [22] and [26], where the the fusion multispectral/hyperspectral was already discussed, the recent works are a step forward. This is the ”Zeitgeist” (spirit of the age or spirit of the time) and it is the reason why some prizes are recognized to different groups for the same invention. In any case, the new term hypersharpening was never introduced in these papers. We can suppose because the background of these other groups was different from ours. Therefore, while this paper was being under review, others were published about fusion multispectral/hyperspectral. In particular in [34] the authors propose to take into account constraints related to the fusion problem via appropriate prior distributions used to build a new Bayesian fusion model. The obtained results are compared with [24] and [26]. Other two up-to-date papers [35] [36] are interesting. Both are based on the same observation model and consider fusion as an inverse problem. They differ for the proposed fusion methods. The first, in fact, relies on the sparse representation. In particular, a sparse regularization term is carefully designed, relying on a decomposition of the scene on a set of dictionaries learned from the observed images; the fusion problem is solved via alternating optimization with respect to the target image and the coding coefficients. The second paper formulates data fusion problem as the minimization of a convex objective function containing two quadratic data-fitting terms and an edge-preserving regularizer.

All the methods previously discussed suffer from a high computational complexity that obliges to process small images. Furthermore these methods are not simple to understand and implement.

Hypersharpening is our solution to the multispectral/hyperspectral fusion problem. Very recently, an important review paper has been published [37] about a comparison of pansharpening methods. In this paper, it is literally stated that ”The focus is on some widely used algorithms following the two main approaches, i.e., spectral and spatial, that are *traditionally* considered for pansharpening: the component substitution (CS) and the multiresolution analysis (MRA)”. In the introduction of this paper we share the same classification (MRA and CS classes) and several of the reviewed methods have been developed by some of the authors.

We are convinced that ”traditionally” does not mean ”old” and ”outdated” but it implies the approaches are consolidated and very effective. Hypersharpening is the effort to lead the traditional pansharpening methods in the fusion multispectral/hyperpectral data. This paper starts to demonstrate that these ”traditional” methods can obtain the same effectiveness that already reach in the pansharpening field.

Hypersharpening is the framework that allows traditional pansharpening methods to be effective to fuse multispectral/hyperspectral data i.e. each hyper-sharpening methodology can be easily implemented as extensions of conventional pansharpening algorithms. Furthermore, we have hopes that the definition of hypersharpening can include all the methods developed for multispectral/hypespectral fusion.

This work presents hypersharpening in its theoretical aspects, by discussing its characteristics deeply. In the pansharpening approaches, the source of the high spatial frequencies is provided a-priori, while in hypersharpening it is object of analysis. In other words, hypersharpening studies how to determine/synthesize the source by which the high spatial frequencies are delivered to obtain the best-fused products, showing that the dimensionality of the input data is relevant.

Following our contribution at WHISPERS 2014 Workshop [38], two variants of the hypersharpening approach are presented. Both variants are experimented on the data set acquired by the improved version of SIM-GA instrument, developed by Selex ES. This instrument is now composed by a Pan camera and two HS sensors. The first HS sensor is in the visible and near-infrared (VNIR) portion of the electromagnetic spectrum and the second one is in short-wavelength infrared (SWIR). The resolution factor is roughly 3 between Pan and VNIR spectrometer and between VNIR and SWIR spectrometers as well. The most important characteristics of SIM-GA are reported in Table I.

Because of instrument configuration, we can use the VNIR hyperspectral bands for (hyper)sharpening the SWIR hyperspectral bands. All the reported experiments demonstrate that the hypersharpening approach is competitive and better than the traditional pansharpening.

This paper is organized as follows.

In Section II we review the issue of the hyperspectral dimensionality since it is relevant for hypersharpening. This discussion is preliminary to the considerations reported in Subsection IV-E.

Section III reports about preprocessing aimed at improving fusion quality. In Section IV, we introduce the hypersharpening approach in general and present two different methods. In Section V, we discuss the importance of system modulation transfer function (MTF) on hypersharpening/pansharpening since it determines the spatial characteristics of the acquired images. Experimental results are reported in Section VI. Conclusions are drawn in Section VII.

II. Dimensionality of hyperspectral data

Hyperspectral data are characterized by a high number of spectral bands. Thus, they are more informative than multispectral at the price of a huge amount of data needed for their representation. This informative content, in spite of being corrupted by the presence of the noise, has properties that, if discovered, allows to represent it in more concise way. Thus, in the scientific literature, specific methods are developed that, by using these characteristics, transform hyperspectral cube in new spaces where the informative content is represented by using less (or much more less) dimensions than the number of original spectral bands.

Among these techniques, Principal Component Analysis (PCA) is one of the first linear technique developed [39]. It is a statistical procedure that uses an orthogonal transformation to convert the HS data into a new data set whose components are linearly uncorrelated. This transformation is defined in such a way that the first principal component has the largest possible variance, whereas each succeeding component has the highest variance possible under the constraint that it is orthogonal to (i.e., uncorrelated with) the previous components.

Minimum Noise Faction (MNF) is another linear transformation that, instead of choosing components to maximize variance, as PCA does, finds non-orthogonal directions that maximize the SNR. This technique can be found in [40], but the implementation integrated in ENVI-IDL follows the exposition presented in [41]. The MNF approach hypothesizes an uncorrelated noise and requires the estimation of the noise covariance matrix. In [42], it is demonstrated that MNF is mathematically equivalent to a sequence of two PCA. The first transformation, applied to the data, decorrelates and rescales the noise based on an estimated noise covariance matrix, obtaining transformed data in which the noise has unit variance and no band-to-band correlation. The second transformation is the standard PCA applied to the noise-whitened data.

Unfortunately, since the noise of remote sensing spectrometers has a component that depends on the signal, the effectiveness of this procedure is questionable [43].

A further method to reduce hyperspectral subspace dimension is proposed in [44]. This approach, named Hyperspectral Signal Identification by Minimum Error (HySime), starts by estimating the signal and the noise correlation matrices, using multiple regression. In this way, it identifies a set of orthogonal directions, of which an unknown subset spans the signal subspace. This subset is then determined by seeking the MMSE between the original signal without noise and a projection of the noisy signal. The paper [44] is also interesting because it contains a deep review of many of the approaches that we are discussing in this section.

In order to reduce dimensionality, an alternative approach is to determine a globally optimal coordinate system for the nonlinear data manifold. Practically, this approach determines a coordinate system that ”follows” the intrinsic shape of the data. One of the most effective method (ISOMAP) is proposed in [45]. This approach relies on graph methods to derive geodesic distances on the high dimensional data manifold. From these distances, a set of intrinsic manifold coordinates that parameterizes the data manifold can be derived. Unfortunately, it is only practical for small datasets, because it is based on a determination of all pairwise distances and minimal path distance that results computationally heavy. In [46] and [47], two ISOMAP variants suitable to process HS data sets are proposed. Both try to overcome the computational problem of the original method; the first adopts a tiling procedure of the original scene while the second, introducing some improvements to the ISOMAP, removes artifacts previously generated and achieves full scene global manifold coordinates. Furthermore, the second variant reduces significantly the computation cost.

All the techniques presented so far, represent the informative content in a more concise way; another interesting approach is selecting from the HS data cube only the small subset of bands that contain almost all the informative content. This method presents the clear advantage that the selected bands are not modified but it requires two different steps: the first is determining the number of the bands that have to be chosen and the second the criterion that selects them.

One of the most interesting approach to determine the band number is HFC, proposed for the first time in [48]. HFC is the acronym of inventor names, i.e., Harsanyi, Farrand and Chang. It first calculates the sample correlation and sample covariance matricies and then finds the difference between their corresponding eigenvalues. Applying a binary hypothesis on this difference and using Neyman-Pearson detector, it establish which eigenvalues of the correlation matrix exhibit significative signal energy.

In a following paper [49], the same authors resume this discussion and introduce the concept of virtual dimensionality (VD). It is defined as the minimum number of spectrally distinct signal sources that characterize the HS data set from the perspective view of target detection and classification. Furthermore, since the HFC method does not have a noise-whitening process, they propose an HFC variant by including a noise-whitening process such that the noise variance in the corresponding correlation and covariance eigenvalues will be the same. Thus, the VD estimation is more accurate.

As proposed in [50], this methodology can be adopted only to determine how many bands need to be selected in order to preserve necessary information, choosing a different method to identify the criterion for band selection. So the authors propose the constrained band selection (CBS) to solve this second issue. It can be considered as a constrained band correlation/dependence minimization approach, which linearly constrains a band while minimizing the correlation or dependency of this particular band with other bands in an HS image. The idea is traced back to the linearly constrained minimum variance (LCMV) developed by Frost in [51].

III. Data set preprocessing

In many papers on pansharpening, the authors draw the readers' attention to the importance of data co-registration. Certainly, it is not possible to perform a good fusion if the data are not registered. Furthermore, we have already demonstrated [2] that the CS and MRA classes have different performances in presence of misregistration problems. In the hypersharpening framework, a further preprocessing is mandatory, that is, the selection of the bands in both the sequences. Generally, in fact, the sequences that can be processed, are provided without excluding the noisy or corrupted bands. When only MS data are involved, this control is less necessary since during the visual analysis of results, all the bands are displayed and so it is simple to discover problems in the original data. Conversely, when HS sequences are involved, not only it is rare that all the bands are displayed but also unprocessable bands are more probable. We would like to point out three factors that lead to obtain noisy or corrupted bands:

- Specific characteristics of the spectrometers. In the SIM-GA VNIR spectrometer the first 20 bands are noisy. This fact is well-known and it is convenient excluding them from the processing.

	Pan	VNIR	SWIR
Spectral range	400 – 1000 nm	400 – 1000 nm	900 – 2500 nm
Spectral sampling	Mono broadband	1.2 nm	5.8 nm
Spectral bands	1	512	256
Spatial pixels	4096	1024	320
IFOV	0.14 mrad	0.5 mrad	1.33 mrad
Ground Sampling Interval @ 1000m altitude	0.167 m	0.5 m	1.5 m

Table I: SIM-GA's characteristics.

- The characteristics of the transmittance of the atmosphere. In some spectral regions, it is so low that the corresponding spectral band does not contain any useful information.
- Problems related to the specific acquisition such as instrument faults and transmission problems.

Thus, we inserted in the work flow a processing block that excludes corrupted bands. For each spectrometer, this block has to exclude the known faulty bands, the bands where transmittance is below a fixed threshold value and the bands that are considered inappropriate after a visual inspection.

In Fig. 1 the atmospheric transmittance is plotted. The yellow color indicates VNIR and SWIR bands of the SIM-GA instrument that are not processed.

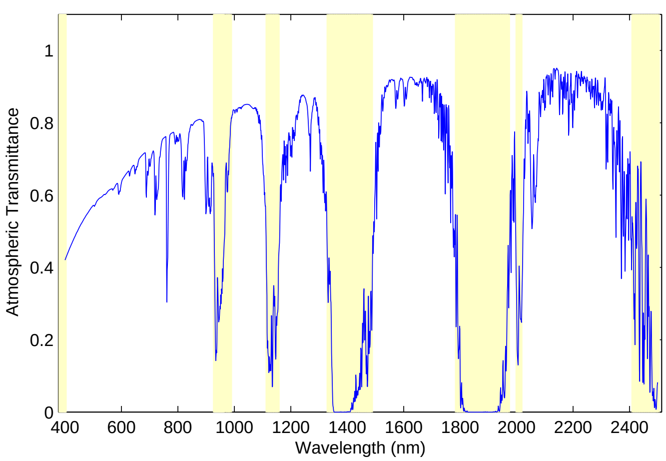

Figure 1: Processed VNIR and SWIR bands.

IV. Hypersharpening

A. General Formulation

In this paper, we present hypersharpening as a new paradigm in remote sensing image fusion. In the traditional approach, the source of high-resolution spatial detail is assigned, while in hypersharpening it is the object of the analysis. In other words, hypersharpening studies how to determine/synthesize the source of spatial details in order to obtain the best fused products. In order to discuss and assess this framework, only one of the most effective methods of pansharpening [52] is used in this paper since our aim is to explore hypersharpening benefits in general and not to compare specific algorithms. This method that belongs to MRA class, adopts Generalized Laplacian Pyramid (GLP) and guarantees a high spectral and spatial quality.

Let use the symbol HS to indicate the original high spatial resolution hyperspectral data at the full scale and the symbol hs to indicate the original low resolution spatial hyperspectral sequence. The number of bands of HS and hs is denoted as M and N, respectively. We also use the symbol $\sim$ to indicate the degraded scale. Furthermore, we use the symbols r and c to indicate the number of rows and columns of HS, respectively. The symbol p is the scale factor between HS and hs. So, let us define:

- $\mathbf{hs} \triangleq \{hs_n, \quad n = 1, \ldots, N\}$ as the original low resolution hyperspectral image.
- $\mathbf{hs}_{exp} \triangleq \{hs_{n_{exp}}, \quad n = 1, \ldots, N\}$ as the $\mathbf{hs}$ image interpolated at full scale.
- $\hat{\mathbf{hs}} \triangleq \{\hat{hs}_n, \quad n = 1, \ldots, N\}$ as the fused $\mathbf{hs}$ image.
- $\mathbf{HS} \triangleq \{HS_m, \quad m = 1, \ldots, M\}$ as the original high resolution hyperspectral image.
- $\tilde{\mathbf{HS}} \triangleq \{\tilde{HS}_m, \quad m = 1, \ldots, M\}$ as $\mathbf{HS}$ at the degraded scale. It is obtained by low-pass filtering and downsampling each band HS_m at the degraded scale.
- $\tilde{\mathbf{HS}}_{exp} \triangleq \{\tilde{HS}_{m_{exp}}, \quad m = 1, \ldots, M\}$ as $\tilde{\mathbf{HS}}$ interpolated at full scale.

Let define now a new entity i.e. the *band* X_n to be derived from $\mathbf{HS}$. X_n indicates, for each band hs_n, the source of spatial detail needed to obtain the fused band $\hat{hs}_n$. $\mathbf{X}$ is the hyperspectral set constituted by all these bands. In conventional pansharpening, X_n is always the panchromatic P, but, in the hypersharpening approach, it can be any band or any modeling of the high-spatial resolution available bands. Furthermore, X_n can be defined according to the specific method developed, thus giving a further degree of freedom to fusion algorithms. Following the previous notation, we define:

- $\tilde{X}_n$ as the band X_n lowpass filtered and downsampled at degraded scale.
- $\tilde{X}_{n_{exp}}$ is the $\tilde{X}_n$ band interpolated at full scale.

So, according to the definition of X_n and the GLP fusion schema presented in [52], we have:

$$\hat{hs}_n \triangleq hs_{n_{exp}} + g_n \cdot (X_n - \tilde{X}_{n_{exp}}) \tag{1}$$

where g_n is a gain factor that can be constant for each pixel in the band or locally computed. In this paper, a global gain is adopted, whose formula is given by:

$$g_n = \frac{cov(hs_{n_{exp}}, \tilde{X}_{n_{exp}})}{var(\tilde{X}_{n_{exp}})} \tag{2}$$

Eq. (1) shows that each fused band is given by adding to the expanded band the weighted sum of the differences between the high spatial resolution source X_n and the band X_n itself, first reduced at degraded scale and then expanded at full scale. These differences represent the injected details.

Although simple, Eq. (1) represents in mathematical form the key difference between pansharpening and hypersharpening, that is, the possibility of specifically designing X_n.

This is the key point of hypersharpening: *given the* $\mathbf{HS}$ *image, taking into account* $\mathbf{hs}$*, process/find/assign, for each* hs_n *band, the most effective/advantageous* X_n *source for fusion*.

The problem of determining $\mathbf{X}$ can be formulated defining the function f that joins $\mathbf{X}$ to $\mathbf{HS}$ and $\mathbf{hs}$:

$$\mathbf{X} = f(\mathbf{HS}, \mathbf{hs}) \tag{3}$$

In other words, we derive $\mathbf{X}$ from $\mathbf{HS}$ according to the spectral and spatial characteristics of $\mathbf{hs}$. In this first study, we simplify Eq. (3) supposing that the following linear model between $\mathbf{X}$ and $\mathbf{HS}$ holds:

$$X_n = \sum_{m=1}^{M} w_{n_m} \cdot HS_m + b_n \tag{4}$$

where the weights w_{n_m} depend on the values of low spatial resolution hyperspectral data sets $\mathbf{hs}_{exp}$ and $\tilde{\mathbf{HS}}_{exp}$.

B. First variant: Selected Band

The first simple criterion proposed in this paper to make Eq. (4) explicit, consists of setting $b_n = 0$ and deriving each X_n by using a single band $HS_{\bar{m}}$; $\bar{m}$ is given by the following formula:

$$w_{n_{\bar{m}}} = \arg\max_m corr(hs_{n_{exp}}, \tilde{HS}_{m_{exp}}) \tag{5}$$

that is, we adopt the $HS_{\bar{m}}$ band that, once degraded and expanded at full scale, exhibits the highest correlation value with $\tilde{hs}_{n_{exp}}$. For this reason, we have

$$w_{n_m} = \begin{cases} 1 & \text{if } m = \bar{m} \\ 0 & \text{otherwise} \end{cases} \tag{6}$$

We label this variant of the hypersharpening approach as *Selected band*.

C. Second variant: Synthesized Band

Before introducing the second criterion, it is necessary to exploit the relationship between $\tilde{X}_{n_{exp}}$ and the linear model introduced in Eq. (4). For simplicity, let us assume that the reduction/expansion operations (low-pass filtering, downsampling and subsequent interpolation) are ideal, so that they can be modeled by only a single low pass filter h. In order to satisfy the Wald's protocol [53] [54], that is, preserve the mean of the signal between the different resolutions, the sum of the coefficients of h has to be equal to 1. If we use the symbol $\star$ for the convolution operation, we have:

$$\tilde{X}_{n_{exp}} = X_n \star h. \tag{7}$$

Inserting the linear model introduced in Eq. (4) into Eq. (7), we obtain:

$$\begin{aligned} \tilde{X}_{n_{exp}} &= \left(\sum_{m=1}^{M} w_{n_m} \cdot HS_m + b_n \right) \star h \\ &= \left(\sum_{m=1}^{M} w_{n_m} \cdot HS_m \right) \star h + b_n \star h \\ &= \sum_{m=1}^{M} w_{n_m} \cdot HS_m \star h + b_n \star h \end{aligned} \tag{8}$$

Since the sum of the coefficients of h is 1, we have:

$$\begin{aligned} \tilde{X}_{n_{exp}} &= \sum_{m=1}^{M} w_{n_m} \cdot HS_m \star h + b_n \\ &= \sum_{m=1}^{M} w_{n_m} \cdot \tilde{HS}_{m_{exp}} + b_n \end{aligned} \tag{9}$$

where

$$\tilde{HS}_{m_{exp}} = HS_m \star h \tag{10}$$

We label this variant of hypersharpening as *Synthesized band*.

D. Implication of Synthesized Band

Since it reasonable that $\tilde{X}_{n_{exp}}$ is as much similar as possible to $hs_{n_{exp}}$, the second hypersharpening criterion estimates, for each hs_n, the set of weights $w_{n_1}, \ldots w_{n_m}, \ldots w_{n_M}$, b_n of Eq. (4) by means of a linear regression algorithm [55], in order to minimize the MSE between $hs_{n_{exp}}$ and $\tilde{X}_{n_{exp}}$.

We would like to draw the reader's attention to the fact that since $\mathbf{X}$ is a high spatial resolution image synthesized by modelling $\mathbf{hs}_{exp}$, it can be also considered a *rough* or preliminary $\hat{\mathbf{hs}}$. In this variant, in fact, each X_n is not selected among a provided set of bands, but it synthesized in such way that $\tilde{X}_{n_{exp}}$ is as similar as possible to $hs_{n_{exp}}$. Thus, X_n, containing almost all the spatial frequency of $hs_{n_{exp}}$, is similar, even though in a rough way, to $\hat{hs}_n$. We interpret this "similar" as the first step of the fusion process. In other words, the synthesized band variant of hypersharpening can be thought of as a two step fusion methodology. In the former step, synthesizing $\mathbf{X}$, we obtain the first rough version of the high spatial resolution image $\hat{\mathbf{hs}}$ and in the latter, applying a traditional fusion methodology (GLP in this paper), we get $\hat{\mathbf{hs}}$.

Furthermore, by inserting Eqs. (4) and (9) in Eq. (1), we demonstrate that the hypersharpening operator $HySharp()$ applied on the generic hs_n band can be expressed as the linear combination of M different pansharpening operators $PanSharp()$ applied to same hs_n band (Eq. (11)). In this way, we can perform M pansharpenings with only one operation, with a significant reduction of processing time. In addition, each m-th detail is processed once and used for all hs_n bands. Modifying some terms in Eq. (11), we believe that future development are possible. We highlight that g_n usually has a dependence on the $\tilde{X}_{n_{exp}}$ term, but in Eq. (11) we consider it independent.

$$
\begin{aligned}
HySharp(hs_n) = \hat{hs}_n &= hs_{n_{exp}} + g_n \cdot (X_n - \tilde{X}_{n_{exp}}) \\
&= hs_{n_{exp}} + g_n \cdot \left(\sum_{m=1}^{M} w_{n_m} \cdot HS_m - \sum_{m=1}^{M} w_{n_m} \cdot \tilde{HS}_{m_{exp}} \right) \\
&= hs_{n_{exp}} + \sum_{m=1}^{M} w_{n_m} \cdot g_n \left(HS_m - \tilde{HS}_{m_{exp}} \right) \\
&= hs_{n_{exp}} \left(1 - \sum_{m=1}^{M} w_{n_m} + \sum_{m=1}^{M} w_{n_m} \right) + \sum_{m=1}^{M} w_{n_m} \cdot g_n \left(HS_m - \tilde{HS}_{m_{exp}} \right) \\
&= hs_{n_{exp}} \left(1 - \sum_{m=1}^{M} w_{n_m} \right) + \sum_{m=1}^{M} w_{n_m} \left(hs_{n_{exp}} + g_n \left(HS_m - \tilde{HS}_{m_{exp}} \right) \right) \\
&= hs_{n_{exp}} \left(1 - \sum_{m=1}^{M} w_{n_m} \right) + \sum_{m=1}^{M} w_{n_m} PanSharp_m(hs_n)
\end{aligned}
\tag{11}
$$

E. Development of Synthesized Band

Let us use the symbol $\tilde{\mathcal{HS}}_{m_{exp}}$ to indicate the column vector $rc \times 1$ composed by all the pixels of the corresponding $\tilde{HS}_{m_{exp}}$ band rearranged by using lexicographical order. At the same way, we use the symbol $\mathcal{hs}_{n_{exp}}$ for the column vector of the corresponding $hs_{n_{exp}}$ band. Furthermore, we adopt the symbol $\mathbf{1}$ for the column vector $rc \times 1$ in which each element is 1.

We define A as the following $rc \times (M+1)$ matrix:

$$
A = \begin{bmatrix} \tilde{\mathcal{HS}}_{1_{exp}}, & ..., & \tilde{\mathcal{HS}}_{m_{exp}}, & ..., & \tilde{\mathcal{HS}}_{M_{exp}}, & \mathbf{1} \end{bmatrix} \tag{12}
$$

Using this notation, we can express the MMSE problem as finding the specific value of the vector $x = \begin{bmatrix} w_{n_1}, & ..., & w_{n_M}, & b_n \end{bmatrix}^T$ that minimizes the following expression:

$$
\left\| \mathcal{hs}_{n_{exp}} - Ax \right\|_2 \tag{13}
$$

where the symbol $\| \quad \|_2$ indicates the 2-norm, that is, the Euclidean norm.

In the MMSE approach, there is no constraint to the value that each weight can assume. In other words, each w_{n_m} can be positive, negative or zero.

In traditional pansharpening approaches, where the MMSE method is used to synthesize an intensity image from the multispectral bands, negative values of w_{n_m} are a discussed issue. A negative value, in fact, is a negative contribution to intensity that being an energy is always positive and should also be the integral of positive contributions. A negative contribution sounds strange, in particular, when the spectral bandwidth of the intensity covers the same range of the multispectral. For this reason, supposing only positive weights can be meaningful.

Conversely, in the hypersharpening context, we use broad or narrow spectral bands to synthesize a single narrow band and, even more important, the spectral range covered by $\mathbf{hs}$ and $\mathbf{HS}$ can be different. For these reasons we don't consider mandatory to constrain w_{n_m} only to positive values. In any case, if not negative weights are requested, we suggest expressing the minimization problem as:

$$
\begin{array}{lll} minimize & \left\| \mathcal{hs}_{n_{exp}} - Ax \right\|_2 & \\ \text{subject to} & w_{n_k} \geq 0 & \text{for } \{k\} \subseteq \{m\} \end{array} \tag{14}
$$

where the expression $\{k\} \subseteq \{m\}$ means that a subset of the weights are constrained to be greater or equal to zero.

Since the objective function and constraints of Eq. (14) are convex, the minimization is a convex optimization problem [56] that can be solved using the software implemented in Matlab®, available at the CVX Research site [57].

Resuming the discussion on the problem minimization expressed in Eq. (13), we have to invert the matrix $A^T A$ to computationally solve it. Some methods are available to do this: Cholesky factorization, QR factorization, and singular value decomposition (SVD). Obviously, the choice of the method depends on the characteristics of the data and in particular of the properties of the matrix A. In the hypersharpening case, since we can suppose a high number of pixels $r \times c$ and a high number of bands M, we can expect that the matrix A is close to be rank-deficient. According to [58], in this specific case, the most valid algorithm is SVD.

Decomposing A by using SVD, we obtain:

$$
A = U \, \Lambda \, V^T \tag{15}
$$

where U is an $rc \times rc$ unitary matrix, Λ is a $rc \times (M+1)$ diagonal matrix with non-negative real numbers in the descending order on the diagonal, and V^T is the $(M+1) \times (M+1)$ transpose of the unitary matrix V. Let us use the symbol λ_i for the i-th diagonal element of Λ. Each λ_i is the i-th eigenvalue of SVD decomposition and the square root of the corresponding eigenvalue of the matrix AA^T.

Furthermore, we define:

$$
cond(A) = \lambda_1 / \lambda_{M+1} \tag{16}
$$

This function, also implemented in Matlab®, can be considered a valid measure of the sensitivity of the solution to the noise of the data. It gives an indication of the accuracy of the results from matrix inversion and the linear equation solution. When this number is significantly greater than 1, the matrix A is close to be rank-deficient. We would like to point out that the operator $cond()$ does not require any information about the characteristics of the noise present in $\tilde{HS}_{m_{exp}}$.

When $cond()$ provides a high value, inverting AA^T by using only the first $\breve{m}$ eigenvalues ($\breve{m} \leqslant M+1$) of SVD, allows obtaining a solution more stable and less influenced by noise. Using only the first $\breve{m}$ eigenvalues, however, has other important implications. To understand them, we introduce the new matrix $\bar{A}$ obtained from A by subtracting to each column its average value. Applying the SVD factorization to $\bar{A}$, we obtain the set of eigenvalues $\{\bar{\lambda}_1, \quad ..., \quad \bar{\lambda}_i, \quad ..., \quad \bar{\lambda}_{M+1}\}$. It is possible to demonstrate the following mathematical relationship:

$$\zeta_m = \frac{\bar{\lambda}_m^2}{M} \tag{17}$$

where ζ_m is m-th eigenvalue of the PCA transformation applied to A.

Thus, the use of the first $\breve{m}$ eigenvalues can be considered equivalent to reduce the dimension of the data by using the PCA transformation. This is a crucial point: in the hypersharpening framework, the representation of the hyperspectral data in a space with a lower dimension has not much importance but, on the contrary, the stability of the minimization expressed by Eq. (13) is of primary importance. In any case, due to Eq. (17), the two goals are substantially equivalent.

Thus, instead of processing the matrix A and choosing a subset of the eigenvalues of the SVD factorization, we can process a new matrix $\breve{A}$ with a reduced number of columns and then use all the eigenvalues of its SVD factorization.

Practically, the definition of $\breve{A}$ is the creation of a new hyperspectral data $\breve{\mathbf{HS}}$ characterized by having less spectral bands. Thus, the definition of hyperspectral data $\breve{\mathbf{HS}}$ is crucial in this new perspective. In this context, the optimal $\breve{\mathbf{HS}}$ is the data that determines the best X_n source of high spatial frequency to hypersharpen hs_n. To sum up, we judge the effectiveness of $\breve{\mathbf{HS}}$ comparing, when it is possible, the fused image $\hat{hs}_n$ with the reference.

We propose in this paper a very simple solution to create $\breve{\mathbf{HS}}$: each band is the not overlapped spectral mean of s bands of $\mathbf{HS}$:

$$\breve{HS}_{m'} = \frac{\sum_{h=m's}^{m's+s-1} HS_h}{s} \qquad m' = 0, 1.., \lfloor M/s \rfloor \tag{18}$$

and we replace HS_m with $\breve{HS}_{m'}$ in Eq. (4).

This simple linear solution has some clear advantages: due to the presence of the mean operator, it reduces at the same time the spectral dimension and the noise. Furthermore, this hyperspectral data set, since it can be considered as a new sequence really acquired with a spectral bandwidth s times the original, reduces the input dimensionality with an approach that can be immediately considered a reasonable solution.

Even if only this simple dimensionality reduction is implement in this paper, we would like briefly discuss about the other techniques already presented in Section II.

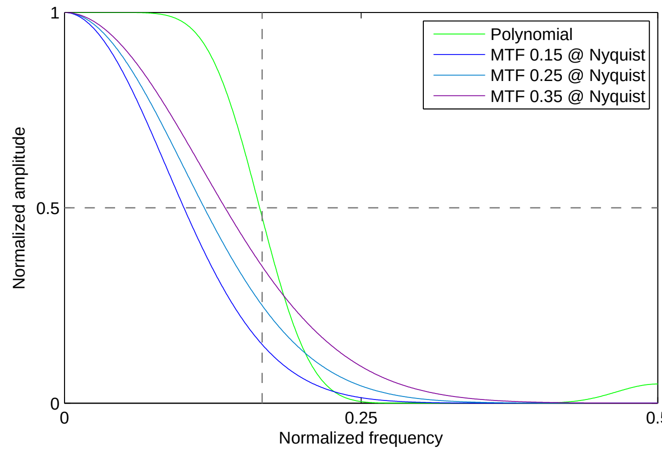

Figure 2: Comparison between the "ideal" spectral response and Gaussian MTFs having different values at Nyquist frequency.

About MNF in addition to difficulties about the estimation of the noise, we would have the problem that the dimension of the matrix A would remain the same. Practically, in hypersharpening, MNF application would be useful only as a denoising procedure of $\tilde{HS}_{n_{exp}}$.

Applying the ISOMAP approach to hypersharpening would be not immediate: it would sound strange that the data were represented by adopting a complex non linear model and at the same time X_n were synthesized by using the simple linear model of Eq. (4). So, a new specific formulation should be developed starting from Eq. (3). We believe that considering ISOMAP in the hypersharpening context would be worth of investigation, even though the real possibility to improve fusion performances is an open issue.

According to , alerea only the small subset of bands that contain almost all the informative content.

The application in the hypersharpening field of the approaches that select specific bands from the HS data cube (Section II) should be valuable. Since, as demonstrated in [50], the number of bands that have to be selected is low, we could create matrix A only using them without any further operations. Unfortunately, since there would be no denoising operation in this way, so the effectiveness would remain at the moment an open issue.

We hope that, even though this discussion is certainly not exhaustive, it can give good suggestions for future works.

V. Hypersharpening vs Pansharpening: MTF is a critical factor

We would like to start by pointing out that pansharpening and hypersharpening use different data as source for the high spatial frequencies. Obviously, the quality of the fused image not only depends on the effectiveness of the applied method but also on the richness of the high spatial frequencies of the source. This last aspect plays a key role when comparing pansharpening and hypersharpening.

It is reasonable to suppose that the Pan has a higher spatial resolution than $\mathbf{HS}$. Let us suppose that in the downsampling procedure, which is necessary to degrade the Pan to the same spatial resolution of $\mathbf{HS}$, we adopt a polynomial filter [7]. Thus, the downsampling operation is equivalent to the assumption that the Pan is acquired by an electro-optic system having the same polynomial modulation transfer function (MTF). Actually, the polynomial filter is a valid approximation of the ideal filter. On the contrary, we reasonably assume that the MTF of each $\mathbf{HS}$ band can be modelled by Gaussian curve.

The adoption of an "ideal filter" determines an advantage in term of richness of high spatial frequencies present in the reduced panchromatic. The Gaussian MTF, in fact, is more selective in frequency than polynomial filter. This is evident by observing Fig. 2, where the spectral response of the polynomial filter with 23 coefficients is compared with Gaussian MTFs having different values at Nyquist frequency. All have the Nyquist frequency at $1/3$ of the signal bandwidth. Obviously, the different amount of high spatial frequencies in the two sources (panchromatic and $\mathbf{HS}$ data) has a key role in the quality of the fused data. In particular, hypersharpening could produce (and indeed produces) a fused image less detailed than pansharpening. This effect, however, is caused by the intrinsic characteristics of the source and does not depend on any weakness of the proposed hypersharpening approach.

This fact has a different implications depending on whether we are in the development or in the operative phase. When we are interested to compare hypersharpening with pansharpening (development phase), the quality of the fused results has not to depend on the quality of the sources. On the contrary, when we are interested in best fusion results (operative phase), we have to provide sources that guarantee the best performance.

Thus, we could find (and indeed we find) a paradox: hypersharpening could result the best fusion approach when the comparison is correctly carried out, but we could be forced to choose pansharpening when the best performances are required.

Future work could overcome this paradox. In a complete processing chain, in fact, the details of the Pan could be used to sharpen the HS source at the scale of the Pan or at the scale of HS, thus introducing the missing spatial details in the HS source.

VI. Results

A. Experiments Setup

The characteristics of SIM-GA instrument (Table I) are particulary suitable to experiment the hypersharpening approach. The instrument is composed by a panchromatic camera and two hyperspectral sensors in the VNIR and SWIR spectral ranges with a resolution factor roughly 3 between Pan and VNIR spectrometer and between VNIR and SWIR spectrometers, respectively. This allows applying hypersharpening to SWIR data using the VNIR sequence. In this way, we can obtain a high resolution SWIR at the spatial resolution of 0.5 m. Due to the presence of the panchromatic also the traditional approach is possible, that is, to pansharpen SWIR data to 0.5 scale. In that case, first the panchromatic has to be degraded from 0.16 m to 0.5 m (VNIR scale). To preserve spatial quality, we low-pass filter the panchromatic by adopting the polynomial filter with 23 coefficients.

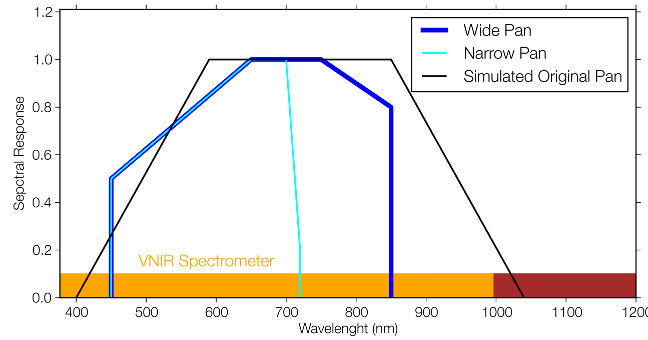

Figure 3: Different spectral responses of Pans.

Two series of experiments are conducted to validate our approach. The first is performed at full scale, that is, the original SWIR data are hypersharpened to 0.5 m; the second, downsampling all the data, is performed at the degraded scale, that is, SWIR data are hypersharpened from 4.5 m to 1.5 m. In this way, the original SWIR data are available as reference for numerical and visual assessment. We compare hypersharpening with the conventional pansharpening approach at both scales.

When pansharpening is performed at the full scale, due to polynomial filter used to downsample panchromatic to 0.5 m, high spatial frequencies are preserved and pansharpening works very well. On the contrary, the performance of hypersharpening depends on the VNIR instrument MTF, that is more selective. Therefore when the results at the full scale are judged and discussed, a great attention has to be devoted to this aspect.

When the fusion is performed at the reduced scale, since all data are downsampled by using the same polynomial filter, there is no influence of filter shape on the quality of the fused products. For this reason, the comparison at the reduced scale is simpler and brings to an immediate recognition of the best approach.

Since in our previous work [59] we demonstrated that the spectral bandwidth of the panchromatic influences the quality of the fused data in the SWIR range, three different panchromatic are synthesized by starting from the VNIR sequence: a narrow (*Narrow Pan*), a wide (*Wide Pan*) and the last with a spectral response similar to the real panchromatic (*Simulated Original Pan*). Their spectral responses are reported in Fig. 3. Incidentally, the real panchromatic is labeled *Original Pan*. We would like to point out, since each panchromatic is synthesized starting from the same VNIR sequence, it can be considered as acquired by an instrument having the MTF similar to the VNIR bands. Thus, the fused results are not affected by the dependence on the difference of the MTFs.

Furthermore, we also report the scores of the expanded images i.e. when the $\mathbf{hs}$ is expanded to $\mathbf{HS}$ scale and no fusion is performed.

To numerically assess the results we adopt RMSE, correlation coefficient (CC), Spectral Angle Mapper (SAM) [60], Erreur Relative Globale Adimensionnelle de Synthèse (ERGAS) [4] and Universal Image Quality index (UIQI) [61]. The

RMSE is normalized to the mean of the reference band.

The adopted dataset is acquired in May 2013 during an airborne survey on Viareggio, Italy. The processed subimages are 378×486 pixels at VNIR scale. The reported RGB images are obtained by choosing the 1071.75 nm band for the red channel, 1647.60 nm for the green and 2191.54 nm for the blue.

B. On parameter s

First, we report on the optimal value of parameter s (Eq. (18)), which determines the subdivision of the bands in the synthesized band hypersharpening.

We report and discuss the results obtained at the reduced scale (1.5 m). In any case, the criterion presented can be adopted to find an effective value of the parameter s also at the full scale where the reference is not available.

We start the discussion reporting in Fig. 4 the values of the eigenvalues of PCA applied to $\mathbf{HS}$. Observing this figure, we conjecture that 19 eigenvalues are approximately sufficient to represent most of the informative content of $\mathbf{HS}$. For this reason, considering Eq. (17), we can also suppose that the first 19 eigenvalues of the SVD applied to matrix A are sufficient to perform the minimum mean square error (MMSE) minimization reported in Eq. (13). Thus, if this hypothesis were true, the best fusion product would be obtained when 19 SVD eigenvalues are used. To verify this, we report in Fig. 5 the ERGAS between hypersharpened and reference SWIR for a different number of SVD eigenvalues. Even though the minimum of the curve is when only 17 eigenvalues are used, we can consider that the obtained results are in good agreement with the initial supposition.

Following the same reasoning, we can suppose that the best $\check{\mathbf{HS}}$ has 19 bands, i.e $m' \simeq 19$. In other words, we hypothesize that we obtain best fusion results when the spectral dimension of $\check{\mathbf{HS}}$ is equal/comparable to the number of significant eigenvalues of PCA. Thus, we compute the value of the parameter s that determines $m' \simeq 19$. Considering that the valid VNIR bands are 467, we find that $s_{optimal} = \lfloor 467/19 \rfloor = 24$. Observing Fig. 6, where ERGAS is reported, even though the minimum of the curve is for $s = 32$, we can notice that the difference between the ERGAS obtained by adopting $s = 32$ or $s = 24$ is not particulary significant. Furthermore, comparing Fig. 5 with Fig. 6, we observe that the minimum values of the two curves are almost the same. In this way, we confirm that choosing the optimal subset of the SVD's eigenvalues is practically equivalent to perform a suitable dimensionality reduction by using $\check{\mathbf{HS}}$ as defined in Eq. (18).

The same conclusion can be reached by comparing the fused images (Fig. 7). We would like to point out that, since X can be considered a first (synthesized) *rough* version of $\hat{\mathbf{hs}}$, all the images reported in Fig. 7 can adopt the visualization map built on the original SWIR image.

Observing Fig. 7(b), it is evident that the Synthesized $\mathbf{X}$ when $s = 1$ is too noisy compared to the original reported in (a). Also in the case of $s = 2$, the results are noisy (c). On the contrary, by using $s = 32$ (d) or only 19 SVD eigenvalues (e), we have two images very similar, less noisy and in good agreement with the original, so that the conclusions of the numerical analysis are strengthened. Furthermore, in Fig. 7(f), we show the image obtained by using only a single eigenvalue; in this case, the figure is monochromatic, even if a reddish color is shown, due to the application of the same visualization map of the others.

As a result of the previous analysis, in the experiments reported hereinafter, we adopt $s = 32$.

C. In-depth of hypersharpening variants

In this subsection, we discuss hypersharpening in more details. In particular, we analyze which bands are chosen in the case of the Selected Band variant, and the values of the weights w_{n_m} regarding the Synthesized Band variant. As in the previous section, the results are obtained at the reduced scale.

In Fig. 8(a), the correlation matrix between VNIR and SWIR data at the scale of 1.5 m and resolution of 4.5 m is represented. The yellow color indicates the bands that are not selected/processed and the magenta points indicate, for each SWIR band, which VNIR band has the maximum value of correlation. According to the definition reported in Subsection IV-C, these bands are used as panchromatics when the selected band variant is adopted. By observing the position of the magenta points, the SWIR shorter wavelengths are more correlated with VNIR longer wavelengths. Instead, starting from 1400 nm, the spectral range of the chosen VNIR bands is near 700 nm.

Observing Fig. 8(b), where we report the histogram of the number of times that each VNIR band is chosen, we notice that few bands are selected many times. Practically, only few bands are useful/informative for selected band hypersharpening. Following the reasoning already exposed in Section II, a future work could propose a new hypersharpening variant where the synthesized bands paradigm is applied only using a subset bands of $\mathbf{HS}$, i.e the $\mathbf{HS}$ bands having most of the occurrences in the histogram.

Regarding synthesized band, in Fig. 8(c) we report the value of weights when MMSE methodology is applied to $\check{\mathbf{HS}}$ and $s = 32$; many values are negative and their physical meaning appears hardly interpretable. Since when $s = 32$, $\check{m} = 14$, that is, $\check{\mathbf{HS}}$ is composed by only 14 bands, we plot the value of the weights of these 14 bands with their central wavelengths. Furthermore, the dynamic range of the weights is significantly greater than one. On the contrary, applying convex optimization with $\check{\mathbf{HS}} = \mathbf{HS}$, that is, $s = 1$ (no spectral reduction) and constraining all weights to be positive or zero, only few bands have significative weights, as shown in (Fig. 8(d)). In other words, the convex optimization uses few bands in the same spectral range of "select bands" (Fig. 8(a)). This is reasonable: by assuming positive weights, the algorithm is forced to use only the most similar bands, that is, the bands with the highest correlation coefficient with respect to the corresponding SWIR band.

For the sake of clarity, Fig. 8(d) displays the zero weight by using the black color.

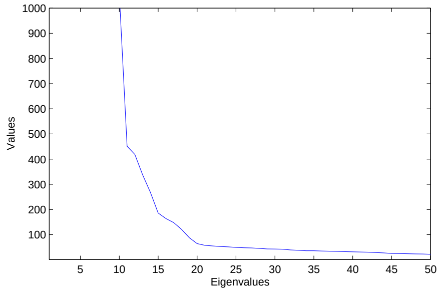

Figure 4: PCA eingenvalues applied to **HS**

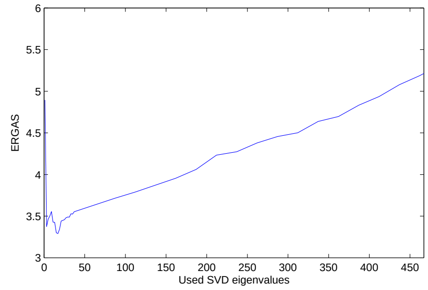

Figure 5: ERGAS comparing fused and original SWIR vs SVD eigenvalues

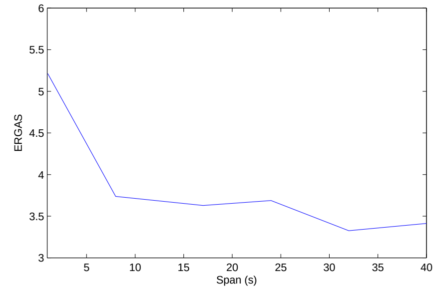

Figure 6: ERGAS comparing fused and original SWIR vs span (s)

(a)

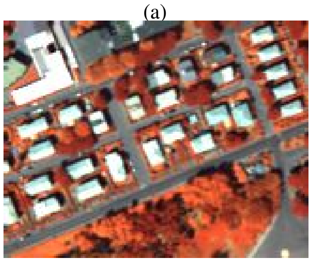

Original SWIR @ 1.5m

(b)

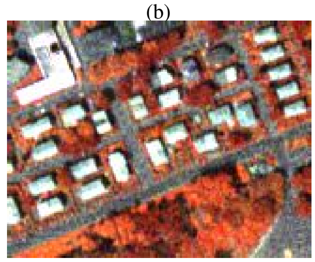

X by using $s = 1$ (Original VNIR)

(c)

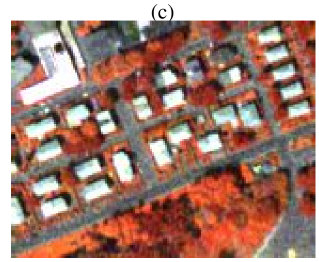

X by using $s = 2$

(d)

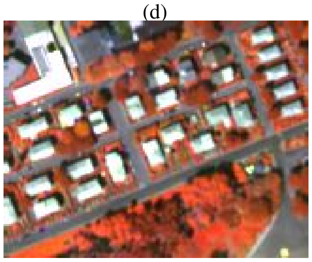

X by using $s = 32$

(e)

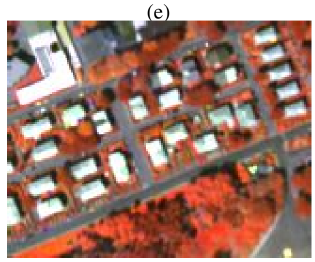

X by using the first 19 eigenvalues of SVD

(f)

X by using only the first eigenvalue

Figure 7: Visual comparison between the original and the synthesized $\mathbf{X}$.

D. Comparison between hypersharpening and pansharpening at the reduced scale

Fig. 9 reports the results obtained at the degraded scale.

We start the analysis by considering Fig. 9(a), which reports the correlation coefficients between $hs_{n_{exp}}$ (expanded SWIR) and the corresponding $\tilde{X}_{n_{exp}}$ band. In the case of Wide Pan, Narrow Pan and Original Pan, $\tilde{X}_{n_{exp}}$ is simply the single panchromatic which is used for all the SWIR bands.

Comparing the different trends, the maximum of correlation value is always obtained by Synthesized Band. Consequently, the best fusion results are obtained by this approach. Fig. 9 reports CC (b), normalized RMSE (c) and UIQI (d).

We would like to draw the readers' attention to the different meaning of Fig. 9(a)and (b): the first score demonstrates that MMSE is effective to synthesize $\tilde{X}_{n_{exp}}$; the second shows that the linear model introduced in Eq. (4) determines the best fusion results. In other words, the fist result can be considered the necessary condition for the second.

Let us focus our attention on Fig. 9(c)(d). Comparing Selected Band with Synthesized Band in the various spectral regions, we can observe that when CC of Fig. 9(a) significantly increases, a corresponding significant improvement occurs in the RMSE and UIQI values.

Furthermore, in the shorter wavelengths of SWIR, Original Pan and Wide Pan perform better than Narrow Pan; on the contrary, in the longer wavelengths, Narrow Pan gives the best results. These trends are coherent with the correlation matrix shown in Fig. 8(a). Since the Narrow Pan does not include the wavelengths which are more correlated with the shorter wavelengths of the SWIR, it performs better in the range $1400 - 2500\ nm$. On the other hand, since these wavelengths are part of the spectral responses of Original Pan and Wide Pan, the performances of these panchromatics in the range $900 - 1400\ nm$ are the best.

The SAM and ERGAS indices reported in Table II confirm that Synthesized Band is the best approach. This table reports also the results obtained by the mode-1 GS-ENVI

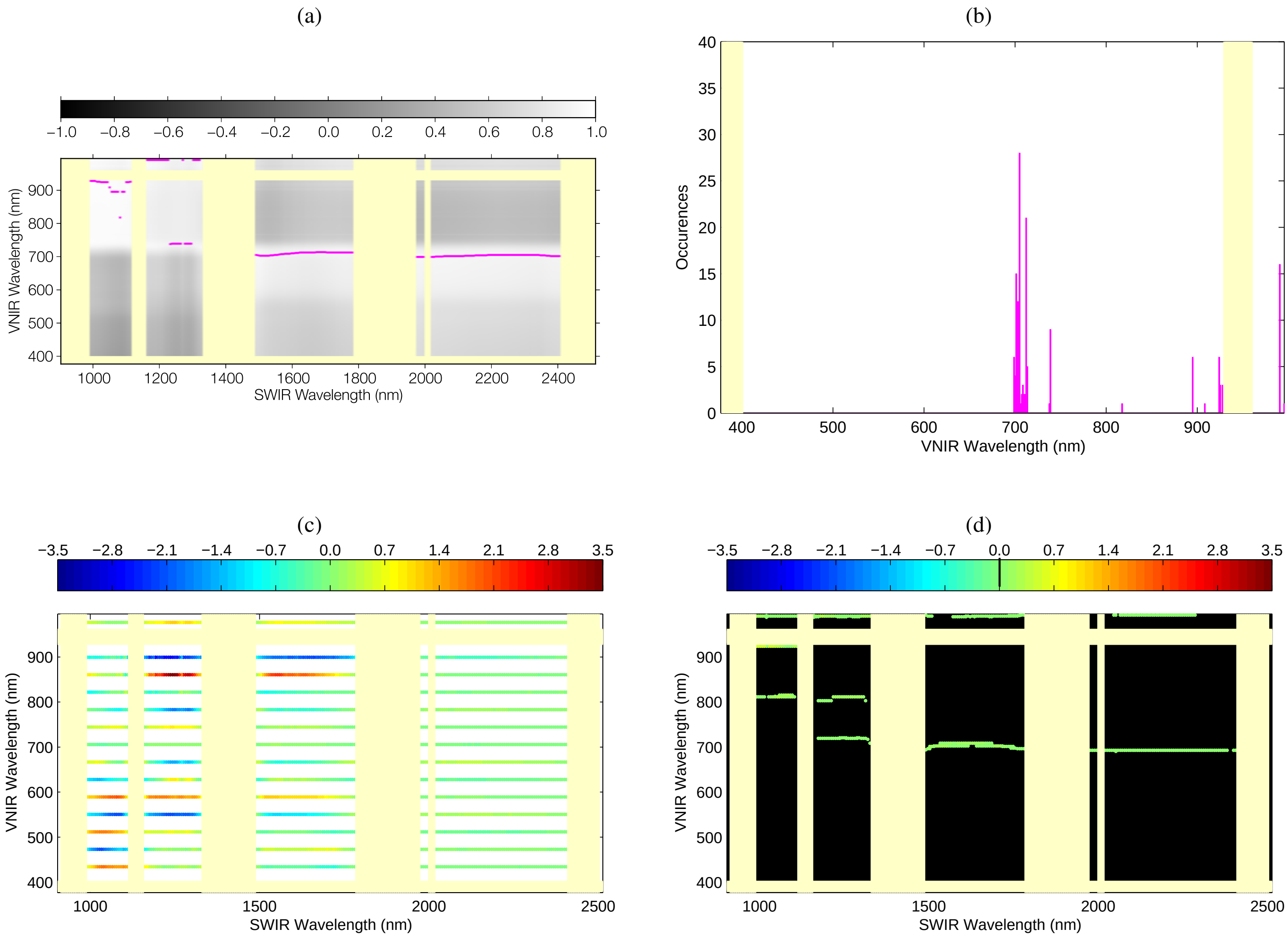

Figure 8: Correlation matrix between SWIR and VNIR data, with the selected bands indicate in magenta color (a); histogram of the times that the bands are selected by the correlation matrix (b); weight values when MMSE is adopted for synthesized band variant with $s = 32$ (c); non negative weight values when convex optimization is adopted for synthesized band variant (d).

implementation, which utilizes the Original Pan as the source of high spatial frequencies. It is evident that the hypersharpening approach exhibits far better performances even if the pansharpening method is good.

E. Comparison between hypersharpening and pansharpening at the full scale

The visual results at the full scale (0.5 m) are reported in Figs. 10, 11 and 12. In these figures, the label ”Original Pan” indicates the Pan reduced to the scale of 0.5 m, whereas the labels ”Selected $\mathbf{X}$” and ”Synthesized $\mathbf{X}$” concern the $\mathbf{X}$ band provided by hypersharpening in selected band and synthesized band modalities, respectively.

A first observation is that in the case of hypersharpening, for each fused band, a display of the specific corresponding source of high frequencies is required. Consequently, Fig. 10(e) and Fig. 10(f) are colored. Fig. 10(e) does not adopt the same visualization map of the others since hypersharpening variant only chooses a specific band of the VNIR sequence. Surely, the application of histogram matching to Fig. 10(e) would make it more similar to the others but we believe that the histogram matching operation would be arbitrary and potentially misleading. Applying this operation, in fact, would make VNIR bands visually more similar to SWIR bands leading to the misinterpretation that VNIR bands are modified to adapt them to the SWIR bands. On the contrary, Fig. 10(f) has the same colors of the expanded and fused SWIR since ”Synthesized Band” variant is aimed at modelling VNIR data as SWIR data.

Observing the ”traditional” Pans, the difference between the Wide (Fig. 10(c)) and the Narrow Pan (Fig. 10(d)) is evident.

We analyze now the fused images reported from Fig. 10(g) to Fig. 10(l). It is evident that the Pansharpened Original Pan (Fig. 10(h)) is the most sharpen image. Furthermore, original Pan degraded at 0.5 m (Fig. 10(a)) is clearly more detailed than the Simulated Original Pan (Fig. 10(b)), which is synthesized from VNIR data using the same spectral response. Thus, following the reasoning exposed in Section V, we can conclude that pansharpening performs better than hypersharpening since VNIR data are acquired with an electro-optic system having a low MTF value @ Nyquist frequency.

Omitting Pansharpened Original Pan from the analysis,

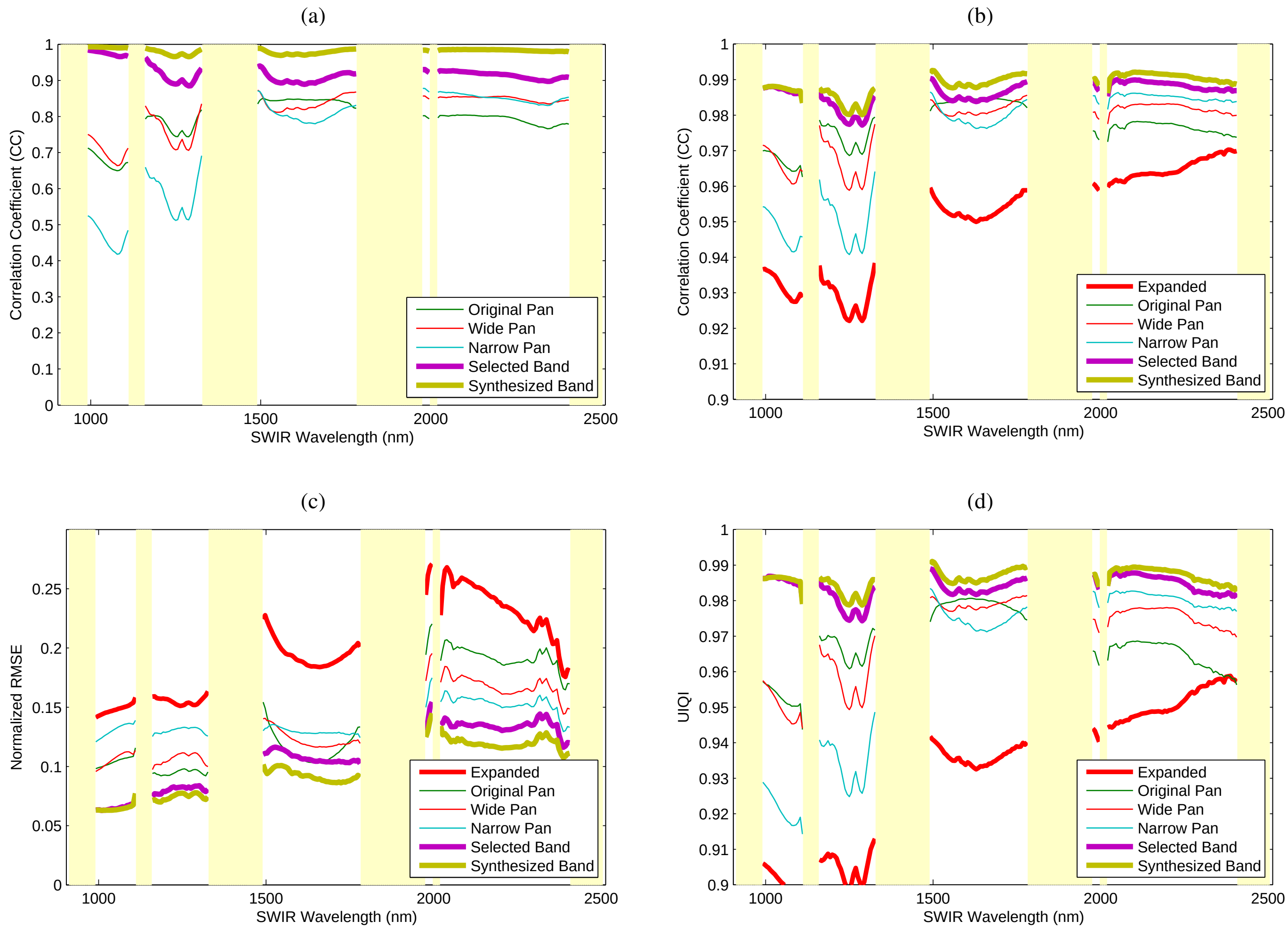

Figure 9: CC between $hs_{n_{exp}}$ and the corresponding $\tilde{X}_{n_{exp}}$ band (a) ; CC between each fusion approach and the reference (b); Normalized RMSE between each fusion approach and the reference (c); Q between each fusion approach and the reference (d).

	Expanded	Pansharpening				Hypersharpening	
		Original Pan	Wide Pan	Narrow Pan	GS-ENVI Orginal Pan	Selected Band	Synthesized Band
SAM	1.98	2.18	2.11	1.82	2.99	1.72	1.51
ERGAS	6.74	4.96	4.67	4.67	10.99	3.73	3.32

Table II: Spectral (SAM) and radiometric (ERGAS) distortions between pansharpened/hypersharpened products and the reference.

fusion results involving similar MTFs can be compared. In this framework, the two variants of hypersparpening approach produce the best fused image (Figs. 10(k) and 10(l)) but with important differences. The ”selected band” variant is less detailed than ”synthesized band” one, as confirmed by the details reported in Fig. 11(l).

On the contrary, the selected band variant does not suffer from local spectral distortions. These ones, in fact, are a possible drawback of the synthesized band variant. Since the weights of the model in Eq. (4) are globally computed, they can produce anomalies on the small details. Observing Fig. 12, in fact, we notice that only the synthesized band variant produces local spectral distortions, that is the anomaly blue spot. To overcome this problem, future works could be devoted to investigate a suitable local model. This development will take into account that the synthesized model could be not effective when the area, where the weights are elaborated, is small.

Both details of Fig. 11 and Fig. 12 confirm that ”synthesized band” produces fused images noisy.

In any case, both variants have a good spatial quality and a valid color fidelity apart from some small details. This confirms the quantitative results at lower scale and justifies the validity of the proposed approach in both variants.

Eventually, in Fig. 13, Fig. 14 and Fig. 15, we compare the spectra obtained at the 0.5 m scale for three different areas:

asphalt, vegetation and roof, respectively. In addition to the original spectrum, the spectra of GS-ENVI Original Pan and of Hypersharpening Synthesized Band methods are plotted. Hypersharpening clearly outperforms GS-ENVI and its spectra are almost indistinguishable from the original ones.

VII. Conclusion

In this paper, we introduce the concept of hypersharpening. Even if we derive it as a natural evolution of pansharpening, hypersharpening could be thought as a new paradigm in remote sensing image fusion.

In this framework, we have proposed two algorithms that have been shown effective on SIM-GA data when hypersharpening the SWIR data by the VNIR sequence, but many other variants could be designed, investigated and developed taking into account that correlation between bands to be fused is crucial.

For sensors with characteristics similar to SIM-GA, hypersharpening can also be the first step to pansharpen the whole datacube, that is, to spatially enhance each band at the resolution of Pan, once the SWIR has been hypersharpened by VNIR. The first step could be seen as a bootstrap strategy aimed at optimizing the second pansharpening step. Since hypersharpening is advantageous with respect to conventional pansharpening, this advantage would obviously reflect on the second step.

Furthermore, when a multispectral sequence would be available together with a lower spatial resolution hyperspectral sequence, hypersharpening by the multispectral sequence would be possible. Future instruments could be designed in order to cope with such an issue and recommendations could be derived for the choice of the spectral width of the high spatial resolution bands.

References

[1] B. Aiazzi, S. Baronti, F. Lotti, and M. Selva, "A comparison between global and context-adaptive pansharpening of multispectral images," *IEEE Geoscience and Remote Sensing Letters*, vol. 6, no. 2, pp. 302–306, April 2009.

[2] S. Baronti, B. Aiazzi, M. Selva, A. Garzelli, and L. Alparone, "A theoretical analysis of the effects of aliasing and misregistration on pansharpened imagery," *IEEE Journal of Selected Topics in Signal Processing*, vol. 5, no. 3, pp. n.a., June 2011.

[3] B. Aiazzi, L. Alparone, S. Baronti, A. Garzelli, and M. Selva, "25 years of pansharpening: a critical review and new developments," in *Signal and Image Processing for Remote Sensing 2nd Edition*, Boca Raton, FL, 2011, pp. 503–548, CRC Press, Taylor and Francis Books.

[4] T. Ranchin and L. Wald, "Fusion of high spatial and spectral resolution images: the ARSIS concept and its implementation," *Photogramm. Eng. Remote Sens.*, vol. 66, no. 1, pp. 49–61, Jan. 2000.

[5] J. Núñez, X. Otazu, O. Fors, A. Prades, V. Palà, and R. Arbiol, "Multiresolution-based image fusion with additive wavelet decomposition," *IEEE Trans. Geosci. Remote Sensing*, vol. 37, no. 3, pp. 1204–1211, May 1999.

[6] X. Otazu, M. Gonzáles Audícana, O. Fors, and J. Núñez, "Introduction of sensor spectral response into image fusion methods. application to wavelet-based methods," *IEEE Trans. Geosci. Remote Sensing*, vol. 43, no. 10, pp. 2376–2385, Oct. 2005.

[7] B. Aiazzi, L. Alparone, S. Baronti, and A. Garzelli, "Context-driven fusion of high spatial and spectral resolution data based on oversampled multiresolution analysis," *IEEE Trans. Geosci. Remote Sensing*, vol. 40, no. 10, pp. 2300–2312, Oct. 2002.

[8] W. Carper, T. Lillesand, and R. Kiefer, "The use of Intensity-Hue-Saturation transformations for merging SPOT panchromatic and multispectral image data," *Photogramm. Eng. Remote Sens.*, vol. 56, no. 4, pp. 459–467, 1990.

[9] T.-M. Tu, S.-C. Su, H.-C. Shyu, and P. S. Huang, "A new look at IHS-like image fusion methods," *Information Fusion*, vol. 2, no. 3, pp. 177–186, Sep. 2001.

[10] A. R. Gillespie, A. B. Kahle, and R. E. Walker, "Color enhancement of highly correlated images–II. Channel ratio and chromaticity transformation techniques," *Remote Sens. Environ.*, vol. 22, no. 2, pp. 343–365, 1987.

[11] V. K. Shettigara, "A generalized component substitution technique for spatial enhancement of multispectral images using a higher resolution data set," *Photogramm. Eng. Remote Sens.*, vol. 58, no. 5, pp. 561–567, May 1992.

[12] T.-M. Tu, P. S. Huang, and P.-Y. Chen, "Blind separation of spectral signatures in hyperspectral imagery," *IEE Proc. Vis. Image Signal. Process.*, vol. 148, no. 4, pp. 217–226, Aug. 2001.

[13] B. Aiazzi, S. Baronti, and M. Selva, "Improving component substitution Pansharpening through multivariate regression of MS+Pan data," *IEEE Transactions on Geoscience and Remote Sensing*, vol. 45, no. 10, pp. 3230–3239, October 2007.

[14] W. Dou, Y. Chen, X. Li, and D. Sui, "A general framework for component substitution image fusion: An implementation using fast image fusion method," *Computers and Geoscience*, vol. 33, no. 2, pp. 219–228, 2007.

[15] D. L. Donoho, "Compressed sensing," *IEEE Transactions on Information Theory*, vol. 52, no. 4, pp. 1289–1306, April 2006.

[16] S. Li and B. Yang, "A new pan-sharpening method using a compressed sensing technique," *IEEE Transactions on Geoscience and Remote Sensing*, vol. 49, no. 2, pp. 738–746, February 2011.

[17] S. Li, H. Yin, and L. Fang, "Remote sensing image fusion via sparse representations over learned dictionaries," *IEEE Transactions on Geoscience and Remote Sensing*, vol. 51, no. 9, pp. 4779–4789, September 2013.

[18] X. X. Zhu and R. Bamler, "A sparse image fusion algorithm with application to pan-sharpening," *IEEE Transactions on Geoscience and Remote Sensing*, vol. 51, no. 5, pp. 2827–2836, May 2013.

[19] H. N. Gross and J. R. Schott, "Application of spectral mixture analysis and image fusion techniques for image sharpening," *Remote Sensing of Environment*, vol. 63, no. 2, pp. 85–94, February 1998.

[20] G.D. Robinson, H.N. Gross, and J.R. Schott, "Evaluation of two applications of spectral mixing models to image fusion," *Remote Sensing of Environment*, vol. 71, no. 3, 2000.

[21] M. T. Eismann and R. C. Hardie, "Application of the stochastic mixing model to hyperspectral resolution enhancement," *IEEE Transactions on Geoscience and Remote Sensing*, vol. 42, no. 9, pp. 1924–1933, September 2004.

[22] N. Yokoya, T. Yairi, and A. Iwasaki, "Coupled nonnegative matrix factorization unmixing for hyperspectral and multispectral data fusion," *IEEE Transactions on Geoscience and Remote Sensing*, vol. 50, no. 2, pp. 528–537, 2012.

[23] N. Yokoya and A. Iwasaki, "Hyperspectral and multispectral data fusion mission on hyperspectral imager suite (hisui)," *International Geoscience and Remote Sensing Symposium (IGARSS)*, pp. 4086–4089, 2013.

[24] R. C. Hardie, M. T. Eismann, and G. L. Wilson, "MAP estimation of hyperspectral image resolution enhancement using an auxiliary sensor," *IEEE Transactions on Image Processing*, vol. 13, no. 9, pp. 1174–1184, September 2004.

[25] M. T. Eismann and R. C. Hardie, "Hyperspectral resolution enhancement using high-resolution multispectral imagery with arbitrary response functions," *IEEE Trans. Geosci. Remote Sensing*, vol. 43, no. 3, pp. 455–465, Mar. 2005.

[26] Y. Zhang, S. De Backer, and P. Scheunders, "Noise-resistant wavelet-based bayesian fusion of multispectral and hyperspectral images," *IEEE Transactions on Geoscience and Remote Sensing*, vol. 47, no. 11, pp. 3834–3843, 2009.

[27] A. Garzelli, L. Capobianco, L. Alparone, B. Aiazzi, S. Baronti, and M. Selva, "Hyperspectral pansharpening based on modulation of pixel spectra," in *Proceedings of the 2nd Workshop on Hyperspectral Image and Signal Processing: Evolution in Remote Sensing (WHISPERS)*, 2010, pp. 1–4.

[28] B. Aiazzi, L. Alparone, S. Baronti, I. Pippi, and M. Selva, "Context modeling for joint spectral and radiometric distortion minimization in pyramid-based fusion of ms and p image data," *Proceedings of SPIE - The International Society for Optical Engineering*, vol. 4885, pp. 46–57, 2002.

[29] L. Alparone, B. Aiazzi, S. Baronti, A. Garzelli, F. Nencini, and M. Selva, “Multispectral and panchromatic data fusion assessment without reference,” *Photogrammetric Engineering and Remote Sensing*, vol. 74, pp. 193–200, 2008.

[30] G. A. Licciardi, M. M. Khan, J. Chanussot, A. Montanvert, L. Condat, and C. Jutten, “Fusion of hyperspectral and panchromatic images using multiresolution analysis and nonlinear pca band reduction,” *Eurasip Journal on Advances in Signal Processing*, vol. 2012, no. 1, 2012.

[31] M.M. Khan, J. Chanussot, L. Condat, and A. Montanvert, “Indusion: Fusion of multispectral and panchromatic images using the induction scaling technique,” *IEEE Geoscience and Remote Sensing Letters*, vol. 5, no. 1, pp. 98–102, 2008.

[32] Z. Chen, H. Pu, B. Wang, and G.-M. Jiang, “Fusion of hyperspectral and multispectral images: A novel framework based on generalization of pan-sharpening methods,” *IEEE Geoscience and Remote Sensing Letters*, vol. 11, no. 8, pp. 1418–1422, 2014.

[33] A. Iwasaki, N. Ohgi, J. Tanii, T. Kawashima, and H. Inada, “Hyperspectral imager suite (hisui)-japanese hyper-multi spectral radiometer,” *International Geoscience and Remote Sensing Symposium (IGARSS)*, pp. 1025–1028, 2011.

[34] Q. Wei, N. Dobigeon, and J.-Y. Tourneret, “Bayesian fusion of hyperspectral and multispectral images,” *ICASSP, IEEE International Conference on Acoustics, Speech and Signal Processing - Proceedings*, pp. 3176–3180, 2014.

[35] Q. Wei, J. Bioucas-Dias, N. Dobigeon, and J.-Y. Tourneret, “Hyperspectral and multispectral image fusion based on a sparse representation,” *IEEE Transactions on Geoscience and Remote Sensing*, vol. 53, no. 7, pp. 3658–3668, 2015.

[36] M. Simoes, J. Bioucas-Dias, L.B. Almeida, and J. Chanussot, “A convex formulation for hyperspectral image superresolution via subspace-based regularization,” *IEEE Transactions on Geoscience and Remote Sensing*, vol. 53, no. 6, pp. 3373–3388, 2015.

[37] G. Vivone, L. Alparone, J. Chanussot, M. Dalla Mura, A. Garzelli, G.A. Licciardi, R. Restaino, and L. Wald, “A critical comparison among pansharpening algorithms,” *IEEE Transactions on Geoscience and Remote Sensing*, vol. 53, no. 5, pp. 2565–2586, 2015.

[38] M. Selva, B. Aiazzi, F. Butera, L. Chiarantini, and S. Baronti, “Hypersharpening of hyperspectral data: a first approach,” in *Proceedings of the 6nd Workshop on Hyperspectral Image and Signal Processing: Evolution in Remote Sensing (WHISPERS)*, 2014, pp. 1–4.

[39] I.T. Jolliffe, *Principal Component Analysis*, Springer Verlag, 1986.

[40] Andrew A. Green, Mark Berman, Paul Switzer, and Maurice D. Craig, “Transformation for ordering multispectral data in terms of image quality with implications for noise removal.,” *IEEE Transactions on Geoscience and Remote Sensing*, vol. 26, no. 1, pp. 65–74, 1988.

[41] F. A. Kruse J. W. Boardman, “Automated spectral analysis: a geological example using aviris data, north grapevine mountains, nevada,” *Procs. ERIM Tenth Thematic Conference on Geologic Remote Sensing*, vol. I, pp. 407–418, 1994.

[42] James B. Lee, A.Stephen Woodyatt, and Mark Berman, “Enhancement of high spectral resolution remote-sensing data by a noise-adjusted principal components transform,” *IEEE Transactions on Geoscience and Remote Sensing*, vol. 28, no. 3, pp. 295–304, 1990, cited By 235.

[43] B. Aiazzi, L. Alparone, S. Baronti, F. Butera, L. Chiarantini, and M. Selva, “Benefits of signal-dependent noise reduction for spectral analysis of data from advanced imaging spectrometers,” *Workshop on Hyperspectral Image and Signal Processing, Evolution in Remote Sensing*, 2011, cited By 0.

[44] J.M. Bioucas-Dias and J.M.P. Nascimento, “Hyperspectral subspace identification,” *IEEE Transactions on Geoscience and Remote Sensing*, vol. 46, no. 8, pp. 2435–2445, 2008.

[45] J.B. Tenenbaum, V. De Silva, and J.C. Langford, “A global geometric framework for nonlinear dimensionality reduction,” *Science*, vol. 290, no. 5500, pp. 2319–2323, 2000.

[46] C.M. Bachmann, T.L. Ainsworth, and R.A. Fusina, “Exploiting manifold geometry in hyperspectral imagery,” *IEEE Transactions on Geoscience and Remote Sensing*, vol. 43, no. 3, pp. 441–454, 2005.

[47] C.M. Bachmann, T.L. Ainsworth, and R.A. Fusina, “Improved manifold coordinate representations of large-scale hyperspectral scenes,” *IEEE Transactions on Geoscience and Remote Sensing*, vol. 44, no. 10, pp. 2786–2803, 2006.

[48] J. Harsanyi, W. Farrand, and C.-I Chang, “Determining the number and identity of spectral endmembers: An integrated approach using neymanpearson eigenthresholding and iterative constrained rms error minimization,” *in Proc. 9th Thematic Conf. Geologic Remote Sens.*, 1993.

[49] C.-I. Chang and Q. Du, “Estimation of number of spectrally distinct signal sources in hyperspectral imagery,” *IEEE Transactions on Geoscience and Remote Sensing*, vol. 42, no. 3, pp. 608–619, 2004, cited By 436.

[50] C.-I. Chang and S. Wang, “Constrained band selection for hyperspectral imagery,” *IEEE Transactions on Geoscience and Remote Sensing*, vol. 44, no. 6, pp. 1575–1585, 2006.

[51] O. L. Frost III, “An algorithm for linearly constrained adaptive array processing,” *Proc. IEEE*, vol. 60, no. 8, pp. 926–935, Aug. 1972.

[52] B. Aiazzi, L. Alparone, S. Baronti, A. Garzelli, and M. Selva, “MTF-tailored multiscale fusion of high-resolution MS and Pan imagery,” *Photogramm. Eng. Remote Sens.*, vol. 72, no. 5, pp. 591–596, May 2006.

[53] L. Wald, T. Ranchin, and M. Mangolini, “Fusion of satellite images of different spatial resolutions: assessing the quality of resulting images,” *Photogramm. Eng. Remote Sens.*, vol. 63, no. 6, pp. 691–699, 1997.

[54] T. Ranchin, B. Aiazzi, L. Alparone, S. Baronti, and L. Wald, “Image fusion - the ARSIS concept and some successful implementation schemes,” *ISPRS J. Photogramm. Remote Sensing*, vol. 58, no. 1-2, pp. 4–18, June 2003.

[55] S. M. Ross, *Introduction to Probability and Statistics for Engineers and Scientists*, ELSEVIER Academic Press, Burlington, MA, 2004.

[56] S. Boyd and L.Vandenberghe, *Convex Optimization*, Cambridge University Press, 2004.

[57] CVX Research, “Cvx: Matlab software for disciplined convex programming,” 2014.

[58] Lloyd N. Trefethen and David Bau, III, Eds., *Numerical Linear Algebra*, 1997.

[59] B. Aiazzi, L. Alparone, S. Baronti, A. Garzelli, and M. Selva, “Pansharpening of hyperspectral images: A critical analysis of requirements and assessment on simulated prisma data,” *Proceedings of SPIE - The International Society for Optical Engineering*, vol. 8892, 2013.

[60] F.A. Kruse, A.B. Lefkoff, J.W. Boardman, K.B. Heidebrecht, A.T. Shapiro, P.J. Barloon, and A.F.H. Goetz, “The spectral image processing system (sips)interactive visualization and analysis of imaging spectrometer data,” *Remote Sensing of Environment*, vol. 44, no. 23, pp. 145 – 163, 1993, Airbone Imaging Spectrometry.

[61] Z. Wang and A. C. Bovik, “A universal image quality index,” *IEEE Signal Processing Lett.*, vol. 9, no. 3, pp. 81–84, Mar. 2002.

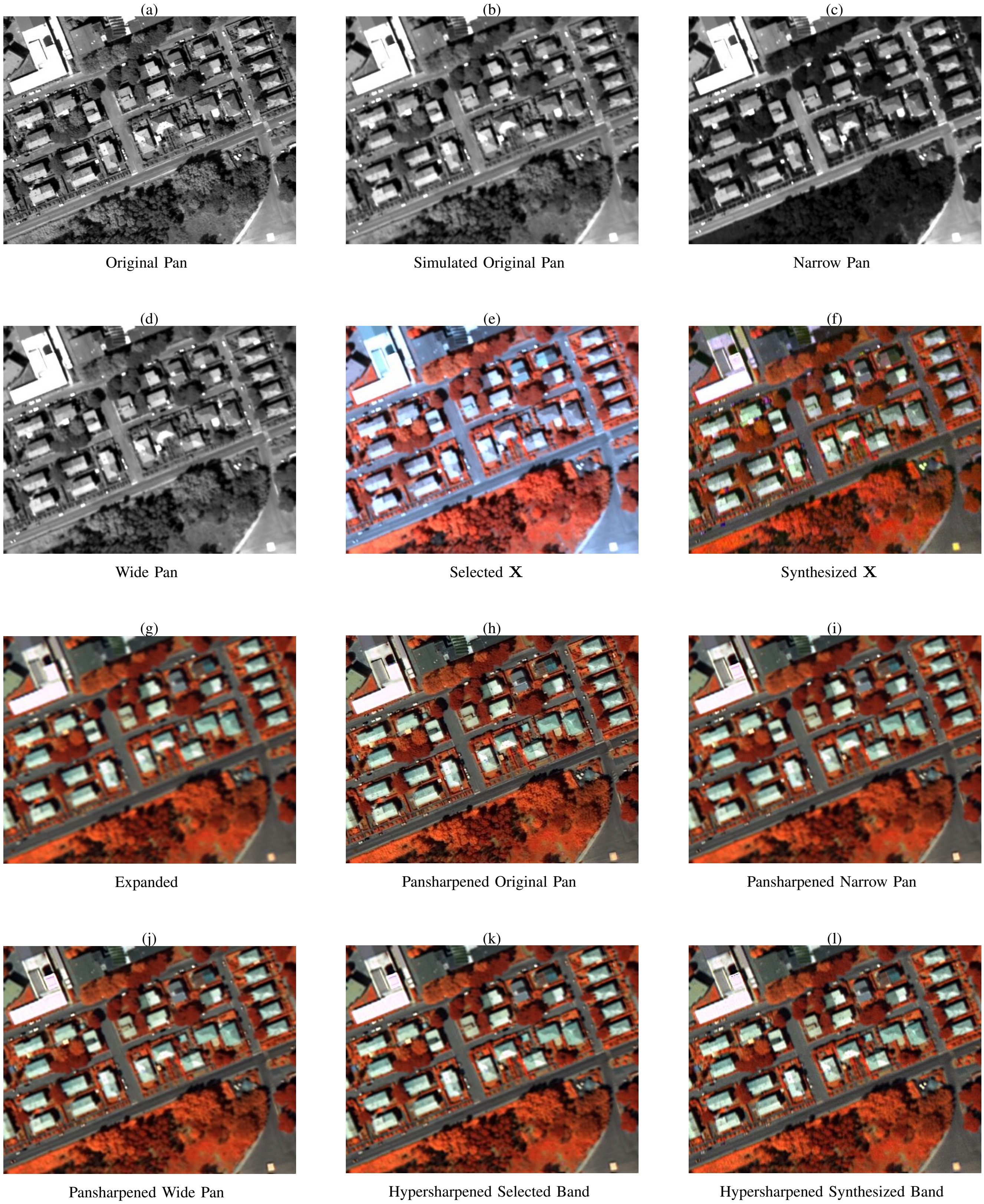

Figure 10: Original, high spatial sources and pansharpened/hypersharpened images produced by the methods experimented at full scale (378×486 at 0.5 m scale).

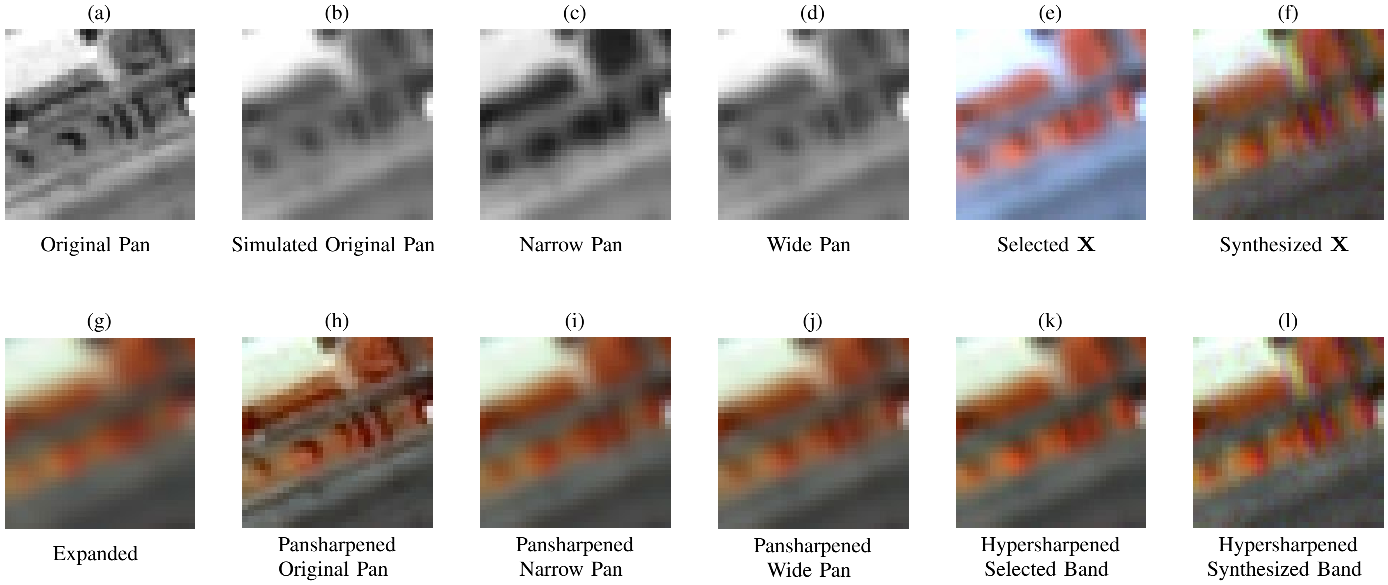

Figure 11: Detail 1 of Fig. 10: local spatial quality (32×32 at 0.5 m scale).

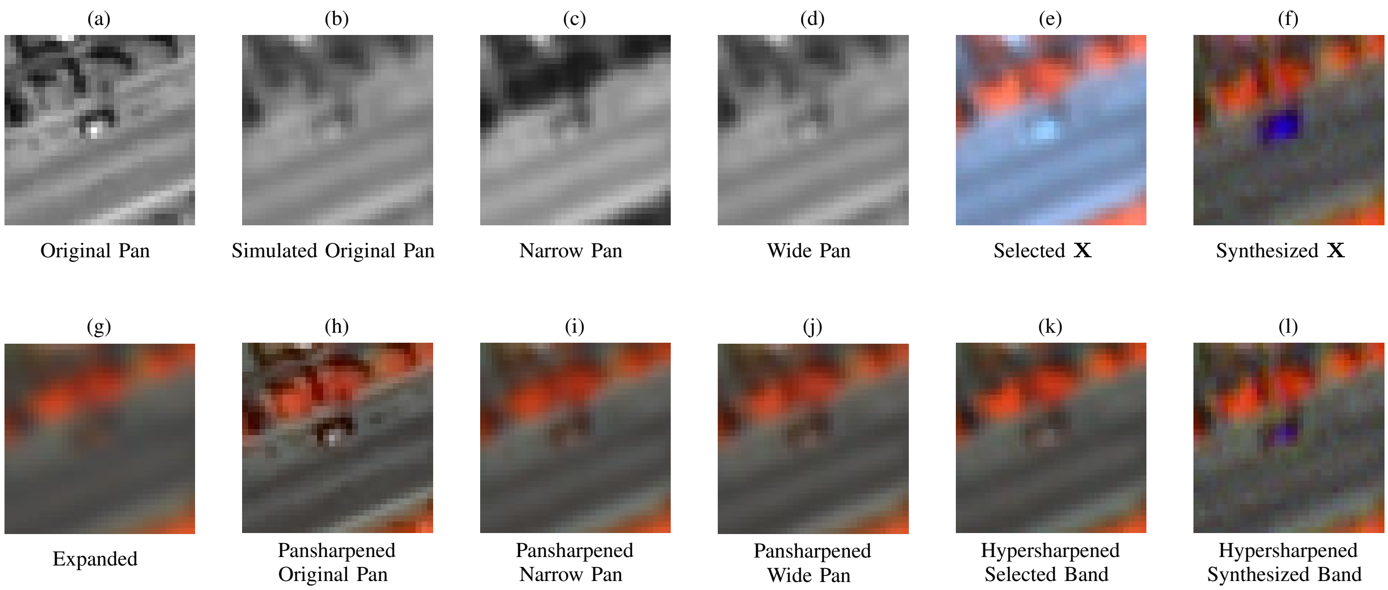

Figure 12: Detail 2 of Fig. 10: local spectral distortion (32×32 at 0.5 m scale).

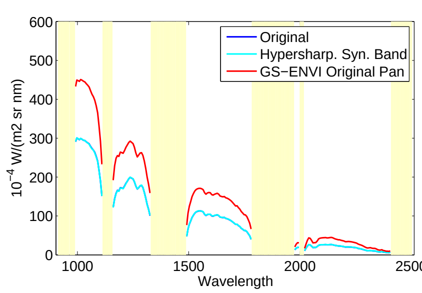

Figure 13: Spectra comparison among fusion methods and original for the *asphalt* area.

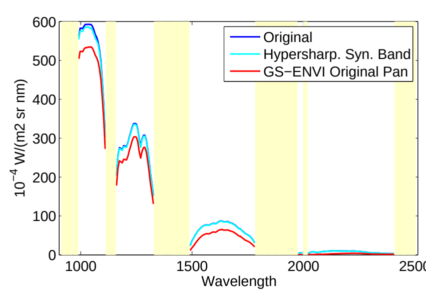

Figure 14: Spectra comparison among fusion methods and original for the *vegetated* area.

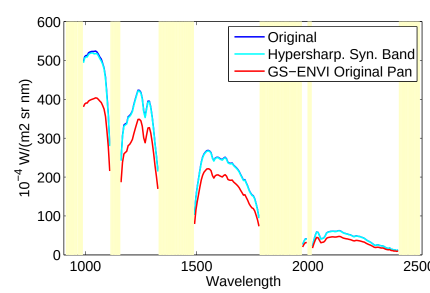

Figure 15: Spectra comparison among fusion methods and original for the *roof* area.